

## DECISION BALANCING: PROCESSES IMPLEMENTATION BASED ON PIR SENSOR PERFORMANCES

Aurelian COSTEA, Paul ȘCHIOPU, Marian VLĂDESCU

Faculty of Electronics, Telecommunications and Information Technology, University "Politehnica" of Bucharest  
Blvd. Iuliu Maniu, 1-3, 061071, Bucharest, Romania  
aureliancostea@yahoo.com

**Abstract:** Along with the technological evolution in the field of infrared sensors and the exponential growth of the complexity of the serviced systems having more and more these sensors as components, it becomes increasingly important to decide with which devices a particular solution will be implemented or with which devices a particular maintenance situation will be solved. More and more devices, components and equipment are available on the supplier market, that claim to have similar sets of functional parameters and reliability. It is increasingly difficult to have a well endorsed scientifically detailed image to correctly, reliably and safely chose between all these devices, components and equipment available nowadays.

**Keywords:** infrared detection, PIR component, wavelength, beamsplitter detector, micro pyramids, plasmonic, driving circuit.

### I. INTRODUCTION

Taking under consideration all data needed (prices, ETA, ETD, etc.), decisions have to be made: what is the best solution that will be implemented, what are the devices, components and equipment selected, most appropriate procedure for implementing the solution.

For security systems, the most common devices used are low speed passive infrared devices, human body detection having the interval of 8-14 $\mu$ m wavelength, usually 10 $\mu$ m.

Knowing and understanding the detailed needs of each of the situations, building step-by-step solutions and implementing them successfully in solving the situations at hand, keeping under control of all possible future evolutions of the system parameters, avoiding the system entering any unwanted or extreme situation, even predicted and documented one, known or not.

The dynamics of processes is basically nonlinear, no two processes have the same evolution path, as well as no process is twice having the same evolution, ideal if possible to have a quasi stable interval of evolution for the complete set of functional parameters.

All objects emit electromagnetic radiation, and the wavelength region over which they emit radiation depends on the temperature of the object. The diagram below shows how the brightness of objects at different temperatures varies

The colder an object is, the longer the peak wavelength of emission.

The electromagnetic spectrum spans a wide range of wavelengths from very short wavelength and highly energetic gamma rays to very long wavelength and low-energy radio waves.

The visible part of the spectrum is only a small portion. Infrared light is the same as the light that we can see except that the wavelength is longer and outside the range that our eyes can sense.

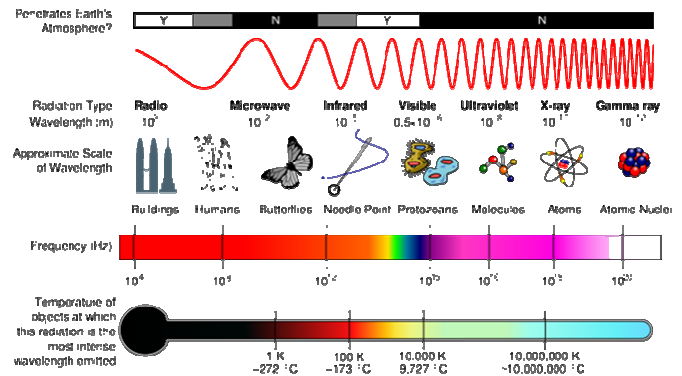


Figure 1. The electromagnetic spectrum.

The Sun has a surface temperature of nearly 6000 Kelvin (where the Kelvin temperature scale is the same as the familiar Centigrade scale except that the zero degrees C is about 273 degrees Kelvin).

Its radiation peaks in the visible part of the spectrum at wavelengths of about half a micron, as shown by the green line in the graph to the right.

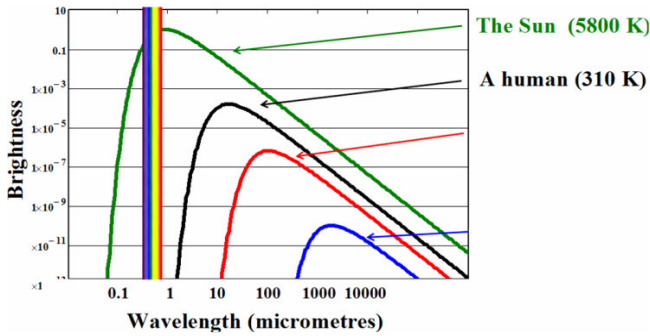


Figure 2. Brightness over wavelength spectrum.

The whole region with wavelengths ranging from 1 micron to 1 mm is loosely called the “infrared”, but scientists tend to break this up into sub-regions: the “near infrared” (from 1 to 5 microns); the “mid infrared” (5 to 30 microns), the “far infrared” (from 30 to 300 microns) and the “submillimeter” (from 300 microns to 1 mm).

The boundaries are somewhat arbitrary, and the exact definitions can vary.

Humans, slightly warmer than room temperature, glow in the mid infrared and we’re brightest at about 10 microns wavelength (black line in the graph).

The pictures below show in visible light (wavelength about 0.5 microns) and infrared light (about 10 microns).

The key difference in these images is that the visible image (Figure 3, top) records short wavelength light (daylight) reflected off his face.

The IR image (Figure 3, bottom) records light that is emitted from his body and clothing, as a result of its temperature.

Note that the light emitted from his face is blocked by his glasses. Glass becomes opaque in the infrared region.



Figure 3. Visible light and infrared light.

Infrared radiation extends from the nominal red edge of the visible spectrum at 700 nanometers (nm) to 1 millimeter (mm).

This range of wavelengths corresponds to a frequency range of approximately 430 THz down to 300 GHz. Below infrared is the microwave portion of the electromagnetic spectrum.

Light comparison			
Name	Wavelength	Frequency (Hz)	Photon Energy (eV)
Gamma ray	less than 0.01 nm	more than 30 EHz	124 keV – 300+ GeV
X-ray	0.01 nm – 10 nm	30 EHz – 30 PHz	124 eV – 124 keV
Ultraviolet	10 nm – 400 nm	30 PHz – 790 THz	3.3 eV – 124 eV
Visible	400 nm–700 nm	790 THz – 430 THz	1.7 eV – 3.3 eV
Infrared	700 nm – 1 mm	430 THz – 300 GHz	1.24 meV – 1.7 eV
Microwave	1 mm – 1 meter	300 GHz – 300 MHz	1.24 μeV – 1.24 meV
Radio	1 meter – 100,000 km	300 MHz – 3 Hz	12.4 feV – 1.24 μeV

Table 1. The wavelength and frequency spectrum.

## II. PYROELECTRIC INFRARED DETECTORS PRINCIPLE SET-UP

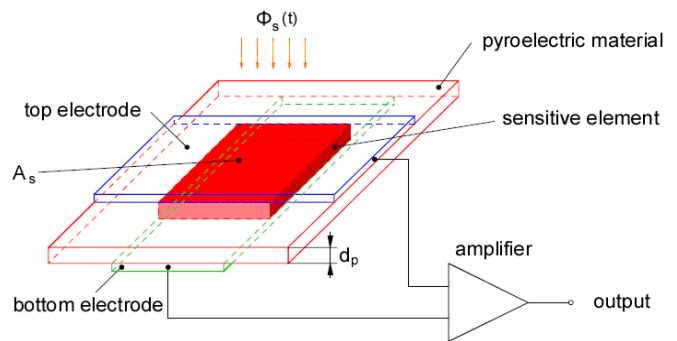


Figure 4. Principle set-up of a pyroelectric infrared detector.

The incident radiation flux  $\Phi_s(t)$  hits the radiation-sensitive element with the area  $A_s$  and absorption coefficient  $\alpha$ .

The absorption of radiation flux results in a temperature change  $\Delta T(t)$  within the pyroelectric material.

The pyroelectric effect generates charges  $\Delta Q(t)$  on the electrodes.

These charges are transformed into a signal voltage  $u_s'(t)$ .

Various noise sources in the pyroelectric chip and the preamplifier generate a noise voltage  $u_R'(t)$  at the detector output.

This voltage limits the radiation flux, which can be detected in the minimum.

## III. DETECTOR CHARACTERISTICS

The essential characteristics of pyroelectric detectors are the responsivity  $S_V$ , the noise equivalent power NEP and the specific detectivity  $D^*$ .

They are defined in the steady-state condition for sinusoidal processes. They generally depend on

modulation frequency  $f$ , wavelength  $\lambda$  and detector temperature  $T$ .

Responsivity  $S_V$  [V/W] is defined as:

$$S_V = \frac{U_S}{\Phi_{\text{rad}}} \quad (1)$$

$\Phi_{\text{rad}}$  rms value of the sinusoidally modulated radiation flux  
 $U_S$  rms value of the sinusoidal signal voltage at the detector output

Noise equivalent power NEP [W] characterizes the signal-to-noise ratio of the detector:

$$\text{NEP} = \frac{U_R}{S_V} \quad (2)$$

$U_R$  rms value of the noise voltage at the detector output

The combination of the equations (1) and (2) shows that the noise equivalent power represents the minimum detectable power of the detector, and is given by a ratio of 1 between signal voltage and noise voltage.

$$(U_S S_V^2)^{-1} / (U_R R^2)^{-1} = 1$$

#### IV. PYROELECTRIC DETECTION TECHNOLOGY

To demonstrate the efficient frequency- and polarization-selective detection, the developed  $15 \mu\text{m}$  absorber was integrated with the commercial discrete pyroelectric sensor.

Originally optimized for sensing IR radiation within the wavelength range of  $2\text{--}20 \mu\text{m}$ , this kind of sensors exhibits the typical voltage responsivity of  $10^5 \text{ V/W}$  at the noise equivalent power (NEP) around  $1.0 \times 10^{-9} \text{ W/Hz}^{1/2}$ .

The basic scheme of the pyroelectric sensor combined with the resonant absorber is depicted in Fig. 5(a).

In this work we attached the resonant absorber directly to the top electrode of the pyroelectric film and fixed it around the periphery by a heat-conducting paste.

The resulting packaged structures are shown in Fig. 5(b).

The absorber's dimensions were correspondingly chosen to be  $2.47 \times 2.30 \text{ mm}^2$  and  $2.47 \times 1.54 \text{ mm}^2$ , that included only  $3 \times 6$  and  $3 \times 4$  resonant patches in the pattern respectively.

From the fundamental point of view, it is of great interest to ascertain the influence of such a small quantity of resonant FSS elements interacting with the incident electromagnetic radiation on the detector performance.

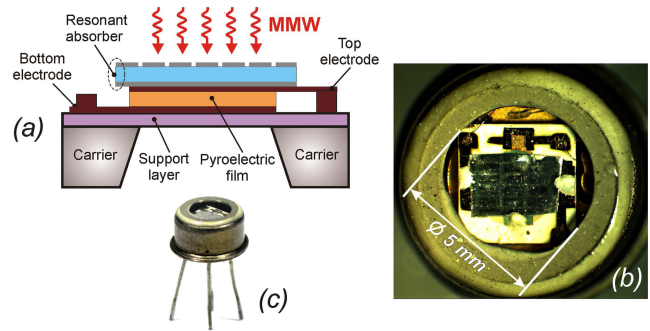


Figure 5. Pyroelectric sensor. (a) Sketch of the pyroelectric sensor with an integrated resonant absorber. (b) Photo of the sensor structure through the sapphire window. (c) Appearance of the accomplished sensor in the standard KT-3 package.

The response time of the pyroelectric detectors was identified via inspecting the time behaviour of the their signals.

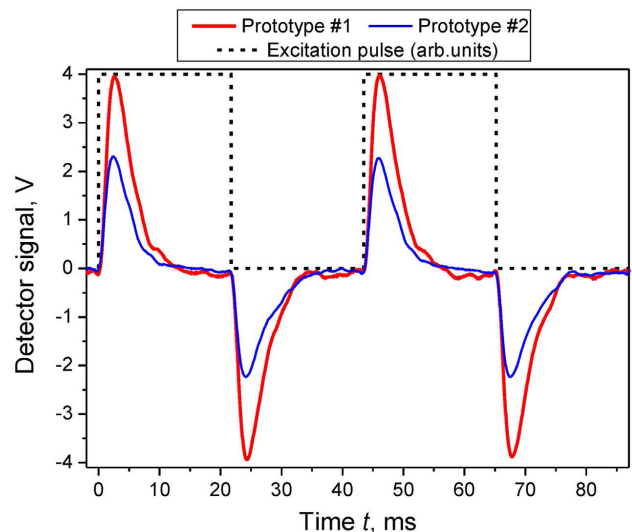


Figure 6. Time response of the pyroelectric detectors with integrated resonant absorbers under meanderpulsed excitation.

A relatively simple and effective approach for selective detection of millimetre waves within a narrow spectral band centred at 140 GHz was shown here by using an ultra-thin near-to-perfect resonant absorber integrated with a compact IR pyroelectric sensor.

Fabricated independently as a self-supporting thin-film metamaterial structure with the wavelength-to-thickness ratio of 136.4, the absorber is realized in a high-impedance surface configuration (FSS-PP-GP) whose ground plane layer is then attached to a top electrode of the pyro-sensor.

As no drastic modification of the original IR sensor is undertaken, excluding substitution of the input window material, such radiation detectors can be produced at relatively low technological expenses.

**V. MICROPHONIC EFFECT IN PYROELECTRIC DETECTORS**

The pyroelectric materials exhibit also piezoelectric behavior then, pyroelectric sensors works also like a piezoelectric sensors.

That's why when the pyroelectric crystal is exposed to a mechanical stress or vibration then the noise signal can be detected. This signal arises from its piezoelectric properties. This phenomenon is called "microphony".

The so called "microphony effect" or acceleration sensitivity strongly depends on the packaging of the sensor chip.

This phenomenon creates unwanted background noise which interferes with the detection of the thermal radiation.

The "microphony" background noise forms part of the signal output from the detector elements to an electronic read-out circuit, and separation of this background noise from the infrared-generated signal component cannot be readily achieved in the read-out circuit.

On the figure you can see response to a referential test that is originally intended for testing piezoelectric sensors.

This test is based on breaking graphite lead against piezo sensor which creates referential wave.

Considering hypothesis that all pyroelectric behave in some cases also like piezoelectric we can declare that there is present noticeable microphony effect on the low frequencies.

All pyroelectric crystals are inherently piezoelectric. When a pyroelectric detector is mechanically excited through shock or vibration, an unwanted signal is produced.

This behavior is called a microphonic effect or vibration response.

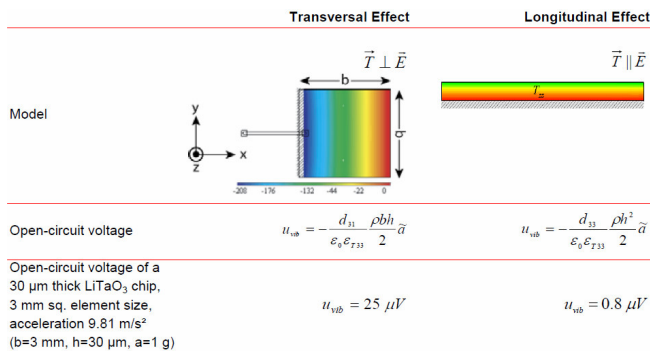


Figure 7. Comparison of transverse and longitudinal effect on a square thin chip.

Microphonic-Equivalent Power (MEP) for a simplified discussion:

$$MEP = \frac{R_{vib}}{R_v}$$

With

$$R_{vib} = \frac{u'_{vib}}{\bar{a}}$$

The MEP is defined as the quotient of the vibration responsivity and voltage responsivity and indicates the incident radiation flux, required to generate an equivalent root-mean-square (rms) signal voltage for a given vibration.

It is expressed in the units of W/g (gravitational acceleration g = 9.81 m/s<sup>2</sup>).

Table 2 summarizes vibration responsivity, voltage responsivity and MEP.

Of course the MEP is more or less independent from the operation mode of the preamplifier.

In the case of a standard detector, the vibration responsivity and hence the MEP strongly depend on the spatial direction of the applied vibration.

In the case of microphonic reduced detectors ('low micro' type) with the novel chip holder, it is clearly demonstrated that the MEP value can be reduced to about (3 ... 2) nW/g @ 10 Hz in all three spatial directions.

Detector	Vibration Responsivity R <sub>vib</sub> (10 Hz, 25 °C) in μV/g			Voltage Responsivity R <sub>v</sub> (500 K, 10 Hz, 25 °C) in V/W without window	Microphonic Equivalent Power MEP (10 Hz, 25 °C) in nW/g		
	x	y	z		x	y	z
LIE-502 (VM)	16	1,6	3,5	160	100	10	22
LIE-500 (CM)	550	55	120	5.500	100	100	22
LME-502 (VM)	0,5	0,5	0,4	160	3	3	2
LME-500 (CM)	65	65	50	22.000	3	3	2

Table 2: Vibration responsivity, voltage responsivity and microphonic-equivalent power of standard and 'low micro' detectors.

In conclusion, there are four ways to reduce the influence of the piezoelectric behavior on pyroelectric detectors:

Suppress mechanical vibrations as much as possible by pulse damper (smooth rubber, flexible cables).

Please note that the elongation [mm] at a constant acceleration [m/s<sup>2</sup>] is frequency dependent.

A sinusoidal acceleration of 1 g = 9.81 m/s<sup>2</sup> is the result of a peak-to-peak elongation of:

70 cm at 1 Hz	7 mm at 10 Hz	70 μm at 100 Hz	0.7 μm at 1 kHz
---------------	---------------	-----------------	-----------------

Table 3: Peak-to-peak elongation at given frequencies.

In a compact sensor module mechanical damping can only be realized for frequencies higher than 100 Hz.

Limit the electrical pass band of the amplifier stages especially at the high frequency side by a steep low pass.

Compensation of the microphonic voltage by sophisticated mounting of the pyroelectric chip.

There are a variety of pyroelectric detectors in voltage mode (VM) or current mode (CM) operation with a reduced vibration response (so called 'low micro') based on mounting technology.

The reduction of the microphonic voltage is in the order of a twentieth (5 %) of a conventional pyroelectric detector.

**VI. BEAMSPLITTER DETECTORS EVEN FOR THE NARROWEST SIGNAL BEAM**

The construction of multi color detectors with integrated beamsplitter is shown in the following picture.

The IR radiation entering through the aperture is divided by a beamsplitter in two or four parts (4 channel

pictured).

Each of the partial beams goes through an IR filter and finally hits a pyroelectric detector chip.

This design works well with single narrow-beam sources or in situations where contamination (dust, insects) in the light path could be an issue.

The beamsplitters are made of gold plated microstructures for the two and four channel devices to achieve a homogeneous distribution of the radiance.

The filters are mounted at a certain angle to obtain a normal incidence of the radiation.

This configuration avoids drifts in the filter transmission curves to shorter wavelengths and the influence of the opposite filter (reflections).

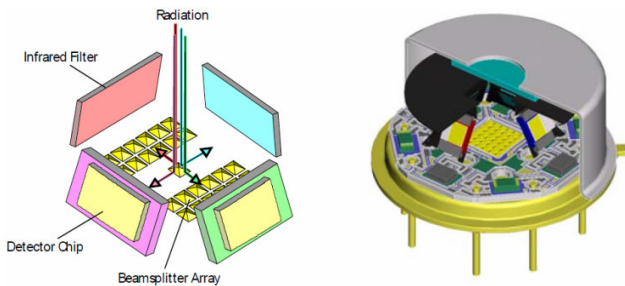


Figure 8: Principle of reflective beamsplittering left side and right side: 3-D Design.

In addition to four channel beamsplitter detectors using four-sided micro pyramids, are also developed two channel detectors based on micro V-grooves.

In the following figure SEM images of two and four channel beamsplitters are shown. The V-grooves pitch is 100 μm and the pyramids are 50 μm, with the tilt angle of the filters and detectors set at 30°.

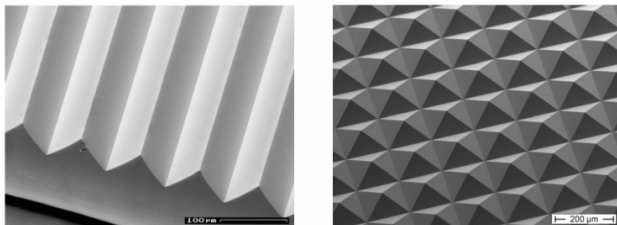


Figure 9: Micro groove (2-channel) and Micro pyramids (4-channel)

Comparison to other multi-channel detectors, the beamsplitter detector has a single aperture compared to conventional multi-channel detectors.

It is possible to use a gas cell with a smaller diameter reducing the gas volume.

A smaller gas volume reduces the size of the sensor module and accelerates the gas exchange.

Also, the signal ratio of all channels is independent from aging, mechanical shift or pollution processes among one another.

The multi-color detectors should be used for the analysis of gas mixtures with few known gases.

Typical examples for a successful application are anesthetic gas monitors and the pulmonary function

testing.

Variable color detectors as described in the following allow a more flexible operation of the analyzer enabling the detection of adjoining or overlapping absorption bands.

In the table3 characteristics of the multi and variable color detectors are summarized.

Detector Specification	Multi Color	Multi Color	Variable Color
Principal	Individual Windows	Beamsplitter	Tunable Fabry-Pérot Filter
Filtering	Parallel	Parallel	Serial
Area to be illuminated	Ø 9.5 mm	Ø 2.5 mm	Ø 1.9 mm
Spectral Range	(2 ... 25) μm	(2 ... 25) μm	(3.0 ... 4.1) μm (3.9 ... 4.8) μm (8.0 ... 10.1) μm
Current Mode (available)	Yes	Yes	Yes
Voltage Mode (available)	Yes	Yes	No
Thermal Compensation	Yes	No	Yes

Table 3: Characteristics of the multi and variable color detectors.

### VII. VARIABLE COLOR DETECTOR

FP filters are fabricated with silicon bulk micromachining technology and wafer bonding.

Bragg reflectors for the specific wavelength ranges are coated on thick silicon carriers to guarantee a high finesse.

The back sides are anti-reflection coated.

The fixed bottom carrier is equipped with control electrodes, whereas the upper reflector is suspended by springs (figure 11).

Applying a voltage  $V_C$  to the electrodes creates an electrostatic force, which decreases the resonator gap  $d$  and, consequently, tunes the filter wavelength.

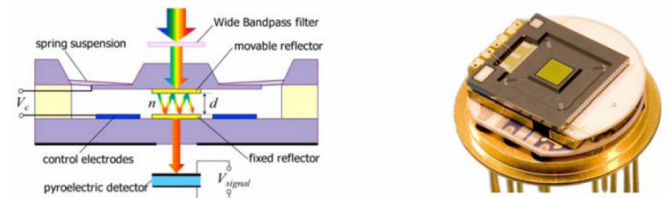


Figure 10: Schematic configuration (left) and picture (right) of the variable color detector.

The MOEMS FPF is integrated in a TO8 housing together with a pyroelectric detector (figure 11).

The latter is a state of the art thermally compensated current-mode type, similar to LME-335 but with smaller feedback capacitance.

This results in a flat frequency response up to several tens of Hz.

The thermal time constant is in the range of 150 ms.

The element size of (2 x 2) mm<sup>2</sup> matches the size of the filter aperture (Ø 1.9 mm).

The broad band pass blocking filter is integrated in the cap.

The mirrors of the FPI are made from dielectric layer stacks (Bragg reflectors) with a limited width of the reflective band (stop band).

The broad band pass and the pyroelectric detector element also show some spectral characteristics.

The spectral response of the detector is a superposition of different fractions, but has to be considered as a whole in the application.

Calibration measurements (figure 12) are performed

by means of an FTIR spectrometer.

The spectra are referenced to a ‘black’ detector with a flat spectral response and normalized to the highest peak (relative spectral response).

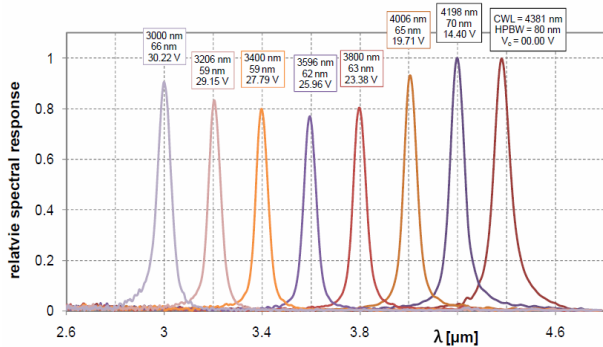


Figure 11: Relative spectral response of a FPF detector LFP-3041L-337 at several tuning voltages.

### VIII. FILTER OPERATION

The filter is electrostatically driven.

The control electrode (V<sub>C+</sub>) is arranged at the fixed reflector carrier, while the movable reflector carrier acts as the counter electrode with the fixed reference potential V<sub>cref</sub> (see Figure 11).

Applying a tuning voltage V<sub>C</sub> = V<sub>C+</sub> - V<sub>cref</sub> results in an electrostatic force F<sub>el</sub> decreasing the electrode gap d<sub>el</sub>.

$$F_{el} = \frac{\epsilon_0 A_{el} V_C^2}{2d_{el}^2}$$

This behavior results in some practical constraints:

The filter is sensitive to acceleration forces: to vibrations (dynamic case) and to the position with respect to the earth’s gravity as well (quasi static case).

Filter settling depends on wavelength.

The filter shows a stability limit at the so-called pull-in point.

This should never be exceeded during operation, otherwise the filter could be damaged.

The filter wavelength can shift with temperature due to thermal expansion of the spacer layer.

Again it should be pointed out, that nearly all parameters, which describe the optical and mechanical behavior of the filter, depend on the mirror position and therefore on the filter wavelength.

The points listed above will be described in more detail in the future sections.

The maximum stable operation range of a voltage controlled electrostatic actuator is therefore limited by the so called pull-in instability.

The pull-in voltage should never be exceeded; otherwise the device may suffer irreparable damage.

In practice this means:

For each individual device (FPF) exists a maximum allowable control voltage for safe and stable operation.

Because of the fabrication tolerances, no general document like datasheets or application notes can provide this information to the user.

One can obtain this from the individual measurement report only.

### IX. DRIVING CIRCUIT

Figure 12 shows a suggestion of a driving circuit for variable color detectors.

Gain and maximum control voltage should be selected according to the filter type.

They can be adjusted through resistors R<sub>2</sub> and R<sub>3</sub>.

The pins Shield, Substrate and V<sub>cref</sub> should be on the same stabilized, low-impedance potential.

Otherwise, spikes, ripples or other interfering signals at these circuit points or the control voltage as well may cause cross talk to the pyroelectric detector due to parasitic capacitances.

The combination C<sub>5</sub> and R<sub>2</sub> form a low pass filter, which helps to reduce voltage transients and therefore to reduce false signals.

The time constant of any electrical filtering should be as high as possible, but should not exceed the mechanical time constant, so that the mechanical filter performance (settling) is not affected.

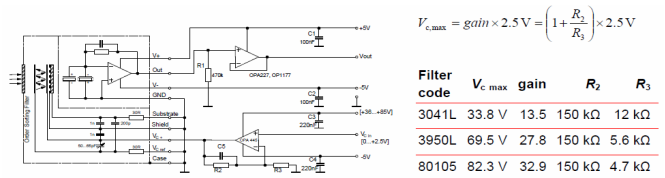
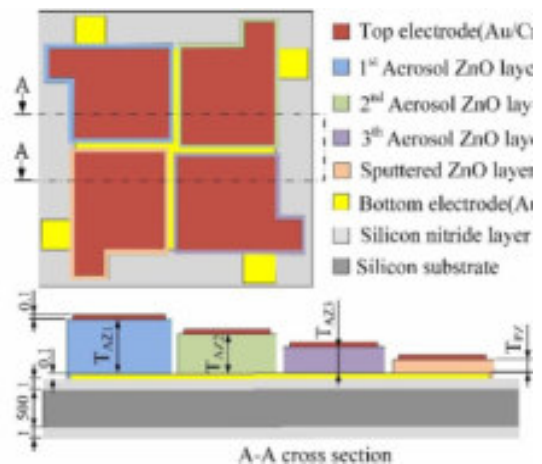


Figure 12: Left: Recommended driving circuit for variable color detectors; right: dimensioning of the filter driving amplifier for several voltage ranges.

All data given in this note show the current stage of Fabry-Pérot product development and various teams constantly works on further improvements which will be published in a suitable way such as updated data sheets.

### X. IMPROVED MULTI-FREQUENCY BAND PYROELECTRIC SENSOR

The improved multi-frequency band pyroelectric sensor - consisting of four ZnO pyroelectric layers with various thicknesses, and top and bottom electrodes, was built on a silicon substrate with a thermal-insulation (silicon nitride) layer to reduce heat and electric loss.



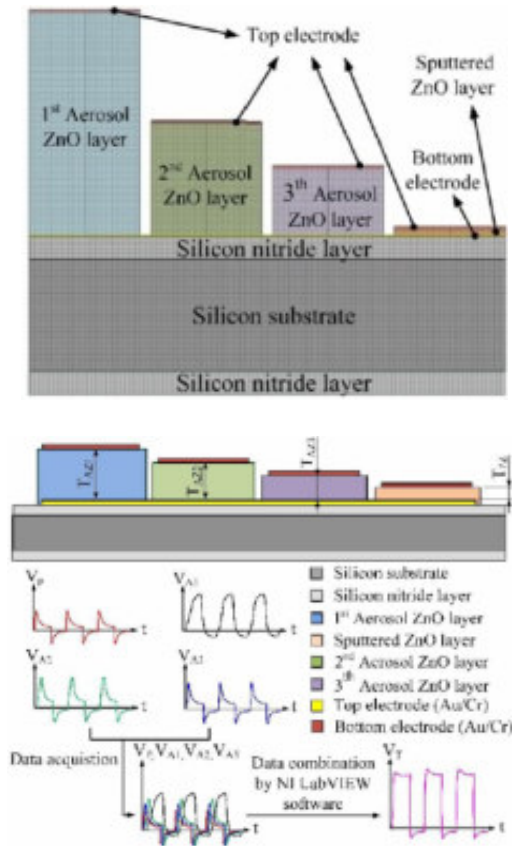


Figure 13: (top) Schematic diagram of the improved multi-frequency band pyroelectric sensor, (center) 2-D model for the improved multi-frequency band ZnO pyroelectric sensor, (bottom) Schematic diagram for electrical signal treatment procedure.

The frequency is very important to distinguish the ranges of low and high frequencies, and the pyroelectric element's thickness determines the value of the thermal time constant ( $\tau T = c \cdot d \times A / GT$ ) under the decided pyroelectric materials and electrode areas.

Therefore, a thicker pyroelectric element increases the thermal time constant, which is suitable as the sensor for a low-frequency range.

Unlike the thicker element, a thinner pyroelectric element reduces the thermal time constant, which is suitable as the sensor for a high-frequency range.

The thinnest ZnO film was deposited by RF sputtering.

Sputter deposited films have a composition close to that of the source material.

Moreover, the thicker ZnO film was grown by the AD.

The AD provides many advantages for producing films in the range of 1~100 $\mu$ m thickness with a high deposition rate, low deposition temperature and low cost.

The AD method can achieve fine patterning and fabricate a dense structure by the reduction of crystallite size by fracture or plastic deformation at room temperature.

The thickness of the sputtered ZnO layer (TPZ) was fixed as 0.3 $\mu$ m, while the thicknesses of the aerosol ZnO layers (TAZ1, TAZ2, TAZ3) were 3, 1 and 0.6 $\mu$ m.

The incident irradiation power applied on the top side of the multi-frequency band pyroelectric device was nearly  $1.228 \times 10^{-12} \text{ W}/\mu\text{m}^2$ .

### XI. PLASMONIC ABSORBERS INFRARED PYROELECTRIC DETECTOR

The hybrid plasmonic-pyroelectric detectors (PA-PIRs) is a device that operates as an uncooled mid infrared detector with narrowband spectral selectivity.

Structured as a ZnO layer sandwiched by a Au microhole array as a top electrode and a Pt bottom electrode as a template for the uniaxially grown ZnO film.

Plasmonic perfect absorbers (PA) is another type of structure which exhibit nearly 100% absorptivity at desired wavelengths.

Plasmonic absorbers have been successfully used in a wide range of applications such as in thermophotovoltaics, photodetectors, molecular sensing and in thermal emitters.

By tuning the geometrical parameters, the absorption band of the PAs can be readily tuned.

Since the infrared light absorbed by a PA is effectively converted into heat, integration of a MWIR PA and a pyroelectric detector is a promising strategy for realizing wavelength-selective devices such as spectroscopic IR sensing and multi-color IR imaging.

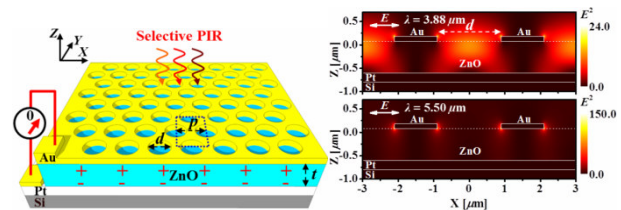


Figure 14: Schematic diagram of the hybrid plasmonic-pyroelectric detectors (PA-PIRs).

In figure above, a schematic diagram of the PA-PIR and geometrical parameters: periodicity - p, Au hole diameter - d and pyroelectric ZnO thickness - t.

The spectra of a PA-PIR (p = 3.0  $\mu$ m, d = 1.8  $\mu$ m, and t = 0.68  $\mu$ m) reveal a dual-band PA resonated at 3.88  $\mu$ m and 5.50  $\mu$ m, which match to two vibrational bands of N<sub>2</sub>O and NO gases, respectively.

Right side - electric field distributions excited at these two resonant peaks.

Electric field polarized in X direction propagates along -Z axis and the amplitude of the incident electric field was normalized to unity.

Absorptivity spectra of PA-PIRs show the tunability of the PA-PIRs by tuning Au hole sizes (1.4, 1.8, 2.4 and 2,7  $\mu$ m) whereas the periodicity and the ZnO thickness are 3.0  $\mu$ m and 0.68  $\mu$ m, respectively for all the four samples.

Our proposed PA-PIR is illustrated in Figure 1a where a hexagonal array of plasmonic Au hole and bottom Pt film is insulated by a ZnO layer.

The thicknesses of Au hole array and Pt films are fixed at 0.1  $\mu$ m and 0.2  $\mu$ m, respectively.

The diameter - d, the periodicity - p of Au hole array, and the thickness - t of the ZnO film were optimized to have a perfect absorptivity in the range of 3 - 7  $\mu$ m (MWIR region) where most of the molecules have their vibrational wavelengths in this region.

The mechanism and detailed optical properties of the tri-layered metal hole-insulator-metal PA have not been discussed here.

## XII. ACKNOWLEDGMENT

The activities presented in this paper were performed in the frame of two programs:

Project PN - III - P1-1.2-PCCDI-2017-0560, "Eco-nano-technologies and smart equipment for mapping the soil parameters and plant growth dynamics in order to increase the efficiency of agricultural production and environmental protection - ENI", under contract no. 41PCCDI/2018, and respectively

Project PN-III-P1-1.2-PCCDI-2017-0419, "Sensors and electronic and photonic integrated systems for the security of people and infrastructures - SENSIS", under contract no. 71PCCDI 2018.

## REFERENCES

- [1] Professional Series Detectors Sensor Data Fusion White Paper (P/N: F01U075616), the Professional Series Detector section of the Bosch web site (<http://www.boschsecurity.us>).
- [2] <https://www.paradox.com/>
- [3] DIAS Infrared GmbH, 2006. <https://www.dias-infrared.com/>
- [4] The DoITPoMS Teaching and Learning Packages are a collection of teaching and learning resources provided for non-profit making purposes within educational institutions <https://www.doitpoms.ac.uk/>
- [5] Chun-Ching Hsiao and Sheng-Yi Liu, "Numerical Analysis for Voltage Responsivities of an Improved Multi-Frequency Band Pyroelectric Sensor," International Journal of Electronics and Electrical Engineering, Vol. 4, No. 1, pp. 39-42, February 2016. doi: 10.18178/ijeee.4.1.39-42
- [6] Thang Duy Dao, Satoshi Ishii, Takahiro Yokoyama, Tomomi Sawada, Ramu Pasupathi Sugavaneshwar, Kai Chen, Yoshiaki Wada, Toshihide Nabatame, and Tadaaki Nagao, "Hole Array Perfect Absorbers for Spectrally Selective Mid-Wavelength Infrared Pyroelectric Detectors". ACS Photonics 2016 3 (7), 1271-1278, DOI: 10.1021/acsp Photonics.6b00249
- [7] H. S. Ahn and K. H. Ko, "Simple pedestrian localization algorithms based on distributed wireless sensor networks," IEEE Trans. Ind. Electron., vol. 56, no. 10, pp. 4296-4302, Oct. 2009.
- [8] K. C. Lee and H. H. Lee, "Network-based fire-detection system via controller area network for smart home automation," IEEE Trans. Consumer Electron., vol. 50, no. 4, pp. 1093-1100, Nov. 2004.
- [9] R. Want, A. Hopper, V. Falcao, and J. Gibbons, "The active badge location system," ACM Trans. Inf. Syst., vol. 10, no. 1, pp. 91-102, Jan. 1992.
- [10] Active Bat. (2008). [Online]. Available: <http://www.cl.cam.ac.uk/research/dtg/attachive/bat/>
- [11] <https://en.wikipedia.org/wiki/Infrared>
- [12] Cuadras, A.; Gasulla, M.; Ferrari, V., "Thermal energy harvesting through pyroelectricity", Sens. Actuators A Phys. 2010, 158, 132-139.
- [13] Hsiao, C.C.; Siao, A.S., "Improving Pyroelectric Energy Harvesting Using a Sandblast Etching Technique", Sensors 2013, 13, 12113-12131.
- [14] Hsiao, C.C.; Siao, A.S.; Ciou, J.C., "Improvement of Pyroelectric Cells for Thermal Energy Harvesting", Sensors 2012, 12, 534-548.
- [15] Whatmore, R.W., "Pyroelectric devices and materials", Rep. Prog. Phys. 1986, 49, 1335-1386.
- [16] Hsiao, C.C.; Liu, S.Y., "Multi-frequency band pyroelectric sensors", Sensors 2014, 14, 22180-22198.
- [17] Porter, S.G., "A brief guide to pyroelectric and detectors", Ferroelectrics 1980, 33, 193-216.
- [18] Hsiao, C.C.; Huang, K.Y.; Hu, Y.C. "Fabrication of a ZnO Pyroelectric Sensor", Sensors 2008, 8, 185-192.
- [19] Hsiao, C.C.; Huang, S.W.; Chang, R.C., "Temperature Field Analysis for ZnO Thin-Film Pyroelectric Devices with Partially Covered Electrode", Sens. Mater. 2012, 24, 421-441.
- [20] Hsiao, C.C.; Luo, L.S., "A Rapid Process for Fabricating Gas Sensors", Sensors 2014, 14, 12219-12232.
- [21] Park, S.H.; Seo, B.C.; Park, H.D.; Yoon, G., "Film bulk acoustic resonator fabrication for radiofrequency filter applications", Jpn. J. Appl. Phys. 2000, 39, 4115-4119.
- [22] Akedo, J., "Aerosol Deposition of Ceramic Thick Films at Room Temperature: Densification Mechanism of Ceramic Layers", J. Am. Ceram. Soc. 2006, 89, 1834-1839.
- [23] Miyoshi, T., "Preparation of Full-Dense Pb(Zr,Ti)O<sub>3</sub> Ceramics by Aerosol Deposition", J. Am. Ceram. Soc. 2008, 91, 2098-2104.